Int J Adv Manuf Technol (2015) 77:1819–1829
DOI 10.1007/s00170-014-6543-7

ORIGINAL ARTICLE

Prediction of grain size and mechanical properties in friction stir welded pure copper joints using a thermal model

A. Heidarzadeh · M. Jabbari · M. Esmaily

Received: 23 August 2014 / Accepted: 22 October 2014 / Published online: 21 November 2014

Abstract In this study, a thermal model was developed and applied to simulate the friction stir welding of pure copper plates with the thickness of 2 mm. The different traverse speeds of 100, 200, 300, and 400 mm min^{-1} and rotational speeds of 400, 700, 900 rev min^{-1} were considered as welding parameters. Microstructural characterization, hardness measurement, tensile test, and fractography were conducted experimentally. The comparison between the numerical and experimental results showed that the developed model was practically accurate. In addition, the results confirmed that the peak temperature was the dominant factor controlling the grain size and mechanical properties, where the fine grains could be achieved at low rotational speed as well as high traverse speed. Consequently, lower peak temperature leads to the high ultimate tensile strength and hardness and the low elongation values.

Keywords Friction stir welding · Copper · Grain size · Mechanical properties · Thermal model

1 Introduction

Special characteristics of copper such as high electrical and thermal conductivities, good combinations of strength and ductility, and excellent resistance to corrosion make it a good candidate to be used in industrial areas. However, conventional fusion welding of copper is somewhat difficult due to issues that the joints experience at the melting point, i.e., high thermal conductivity, large distortion, solidification cracking, and high oxidation rate. Fortunately, the friction stir welding (FSW) has the capability to solve the problem associated with the welding of copper and copper alloys [1–3].

Although many efforts have been made on FSW of aluminum alloys, investigations in the FSW of the copper and copper alloys are relatively limited. This limitation is due to the high melting point and the high thermal conductivity of the copper which require more heat input to produce defect-free joints. Recently, some researchers have studied the microstructures and mechanical properties of the friction stir welded copper [4–15]. For example, Xie et al. [4] achieved defect-free joints of pure copper at low heat input conditions, and they also found that the grain size of the stir zone (SZ) decreases from 9 to 3.5 μm by decreasing the rotational speed. They, moreover, indicated that the microhardness and the yield strength of the SZ vary with the grain size through the Hall-Petch relationship. Similarly, Sun et al. [7] developed a process window for FSW of the copper, and showed that the sound joints can be achieved at the traverse speeds ranged between 200 and 800 mm min^{-1}, the rotational speeds ranged between 400 and 1,150 rev min^{-1}, as well as the applied loads ranged between 1,000 and 1,500 kg. They elaborated that increasing the axial load has a more profound effect on reduction of the SZ grain size compared to decreasing the rotational speed.

FSW parameters such as rotational and traverse speeds of the tool influence the mechanical properties of the joints. Thus, it is necessary to reach the best mechanical properties by optimizing the FSW parameters. One way to optimize the FSW parameters is using statistical equations which are obtained from experimental results. For example, some

A. Heidarzadeh (✉)
Young Researchers and Elite Club, Ahar Branch, Islamic Azad University, Ahar, Iran
e-mail: a_heidarzadeh@sut.ac.ir

M. Jabbari
Department of Mechanical Engineering, Technical University of Denmark, Nils Koppels Allé, 2800, Kgs. Lyngby, Denmark

M. Esmaily
Department of Chemical and Biological Engineering, Chalmers University of Technology, SE-412 96 Gothenburg, Sweden

researchers have used response surface methodology (RSM) to optimize the FSW parameters [16–22]. Heidarzadeh et al. [19, 20] have predicted the mechanical properties of the friction stir welded pure copper plates with different thicknesses of 2 and 5 mm. They have developed the statistical models to predict and optimize the mechanical properties of the joints using Design Expert software. Unfortunately, the main disadvantage of these statistical methods is the need for a large number of trial experiments which consume time and cost.

Another way to optimize the mechanical properties of the FSW joints is to model the process numerically and predict the microstructural changes in the SZ. According to the literature [4–15], it is obvious that grain size of the SZ has the most important role in mechanical features of the joints. Therefore, predicting the final grain size of the SZ using a numerical model will help to control the mechanical properties of the joints. It is notable that the predicted optimum condition can be influenced by FSW parameters like the traverse and the rotational speeds of the tool, plate thickness, alloy composition, tool design, etc.

Although FSW is simple in concept, the physics behind the process is complex, including mechanical heat generation, heat, and mass transport. The large strains and strain rates prevent observing the details of the process, which makes the modeling process attractive or/and essential for understanding it [23–26]. For the limited extent of the plate width, most of the previous models were developed analytically in order to formulate the heat generation, as a point source or line source [27–29].

FSW involves a severe plastic deformation (SPD) and dynamic recrystallization (DRX) in the SZ due to the stirring action of the tool pin together with the elevated temperature (due to the heat generation). The efficient method to simulate the aforementioned phenomena is to develop a thermomechanical model, which accounts for coupled thermomechanical constitutive behavior of the joints. Such models have been developed and used for FSW of Al alloys in literatures [30, 31]. However, finding a correct constitutive model for simulation of the flow behavior of the copper alloys in the elevated temperature has not been introduced in literature, yet navigating the research towards the use of analytical and thermal models.

The thermal model developed in this study is based on the model introduced by Song and Kovacevic [32] for the moving coordinate system. They showed that the grain size increases with increasing of the rotation speed at a constant traverse speed. In this study, the developed thermal model is used to predict the grain size of the SZ in friction stir welded joints of an oxygen-free high conductivity (OFHC) copper with 2 mm thickness. Both the rotational and traverse speeds were considered as the welding parameters. These two parameters play an important role in the amount of the total heat input applied during the process, however, this phenomenon is mostly analyzed qualitatively and the conclusions have been made based on the resultant weld defects. Therefore, the optimum range of the rotational and traverse speeds will be an important parameter to achieve high quality weld, since the variation of these parameters will affect the thermomechanical condition for the microstructural changes in the specimen. The thermal modeling of the friction stir welding of OFHC copper is conducted with the commercial finite element code (COMSOL), and the generated heat is used for modeling the grain growth in the SZ. The results of numerical modeling are compared with the results obtained by corresponding experiments.

2 Experimental methods

2.1 Mathematical model

The heat flux in FSW is primarily given by:

$$\rho c_p T + Q^{\text{gen}} = \nabla \cdot k \nabla T \tag{1}$$

where Q^{gen} is the volumetric heat source term arising from plastic dissipation (W/m^3), ρ is the density of materials, C_p is the mass specific heat capacity, k is the coefficient of thermal conductivity, and T is the temperature.

Tool movement during the process would require a fairly complex model as a moving heat source. Based on the previous work [32] a moving coordinate system is used in the present study, which is fixed at the tool axis. In order to simplify the model, the coordinate transformation assumes that the copper plates are infinitely long (see Fig. 1). This means that the analysis neglects effects near the edges of the plates. Neither does the model account for the stirring process in the copper and material flow from the front to the back of the rotating tool. Moreover, the model geometry is symmetric around the weld. It is therefore sufficient to model only one copper plate. Fixing the coordinate system, thus changes the heat flux (Eq. 1) taking account for the conductive term, as follows:

$$\nabla \cdot (-k \nabla T) = Q - \rho c_p u \cdot \nabla T \tag{2}$$

where u is the velocity of the tool.

The heat generated at the interface between the tool pin and the workpiece as a surface heat source is modeled as below [32]:

$$q_p(T) = \frac{\mu}{\sqrt{3(1+\mu^2)}} r_p \omega Y_{av}(T) \tag{3}$$

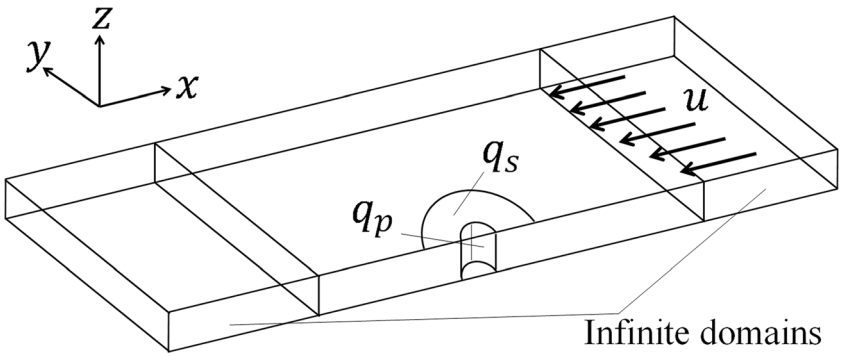

Fig. 1 Schematic illustration of the geometry used in this paper

where μ is the friction coefficient, r_p is the pin radius, w denotes the pin angular velocity, and Y_{av} refers to the average yield stress of the material. The average yield stress, as a function of the temperature, is approximated with an interpolation function determined from experimental data [33] shown in Fig. 2.

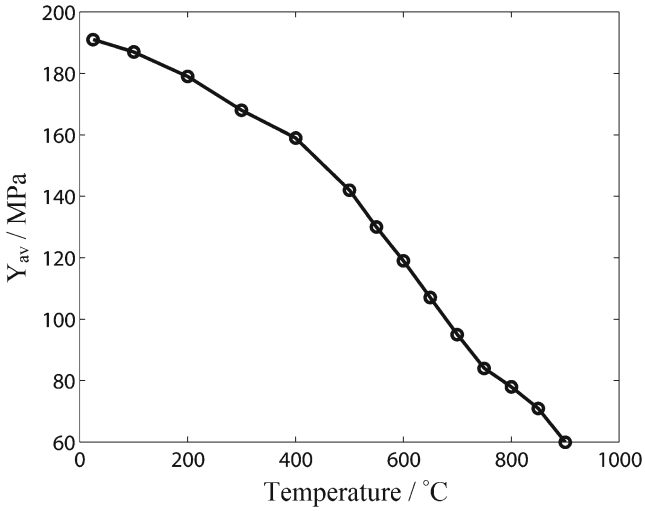

Fig. 2 Interpolation representing yield stress (MPa) vs. temperature (°C) for pure copper

The heat at the interface between the shoulder and the workpiece is formulated by the local heat flux per unit area (W/m^2) at the distance r from the center axis of the tool:

$$q_s(r,T) = \begin{cases} (\mu F_n/A_s)\omega r & T < T_{\text{melt}} \\ 0 & T \geq T_{\text{melt}} \end{cases} \quad (4)$$

where F_n represents the normal force, A_s is the shoulder surface area, and T_{melt} is copper melting temperature.

For initial grain size G_i and final grain size G_f, the energy Q released by grain growth is:

$$Q = 3\gamma\left(\frac{1}{G_i} - \frac{1}{G_f}\right) \quad (5)$$

Where γ is the areal energy density of grain boundary and is equal to 0.5 J m^{-3} for Cu [34]. In this study, the Eq. 5 is modified and used for the grain growth through the generated heat during the FSW process.

2.2 Experimental details

OFHC copper plates of 50 mm wide, 100 mm long, and 2 mm thickness were used as a base material (BM). These plates

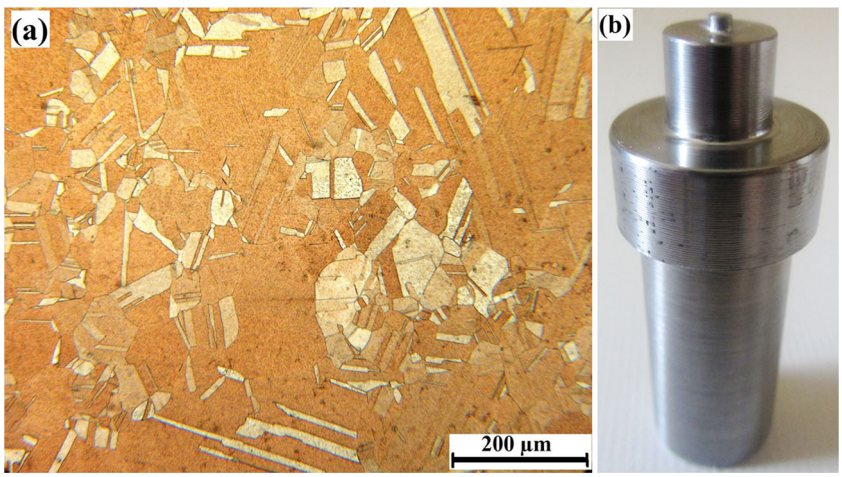

Fig. 3 **a** The microstructure of BM, and **b** The utilized FSW tool

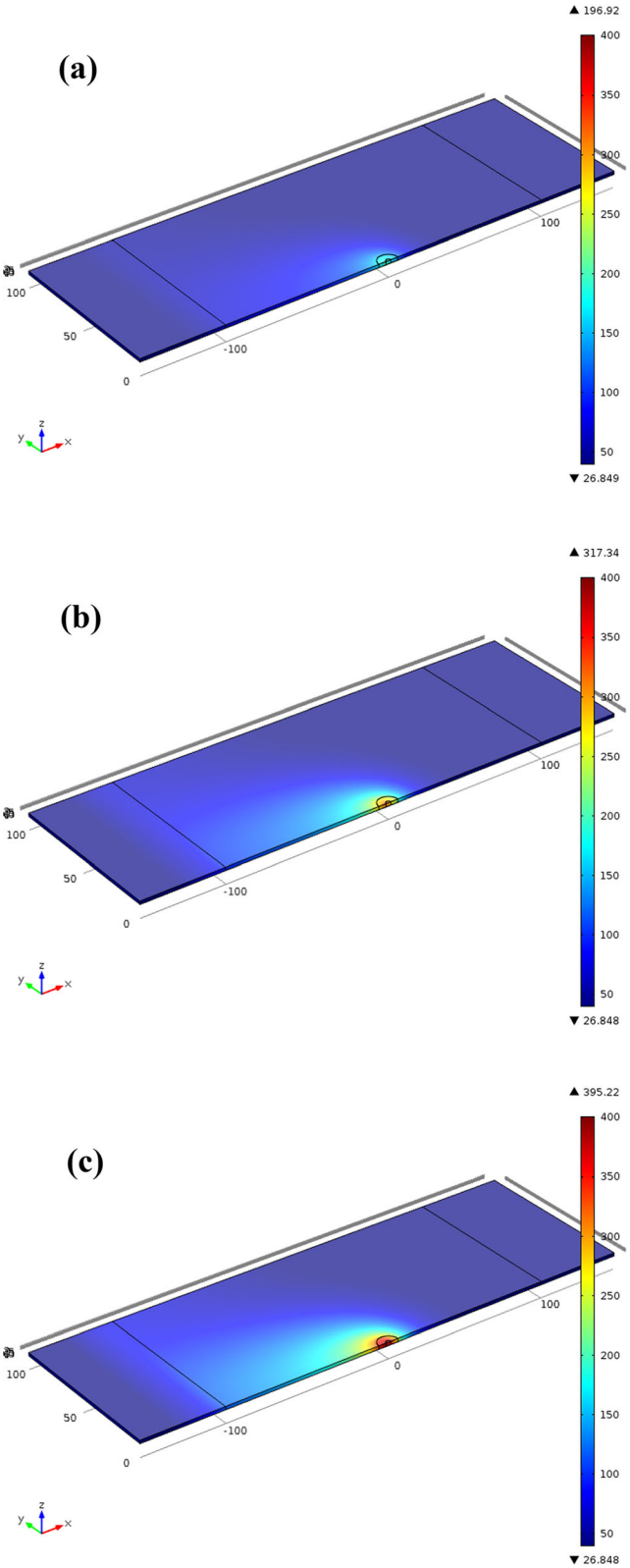

Fig. 4 Temperature distribution in the weld with the traverse speed of 400 mm min^{-1} and the rotational speed of **a** 400 rev min^{-1}, **b** 700 rev min^{-1}, and (**c**) 900 rev min^{-1}

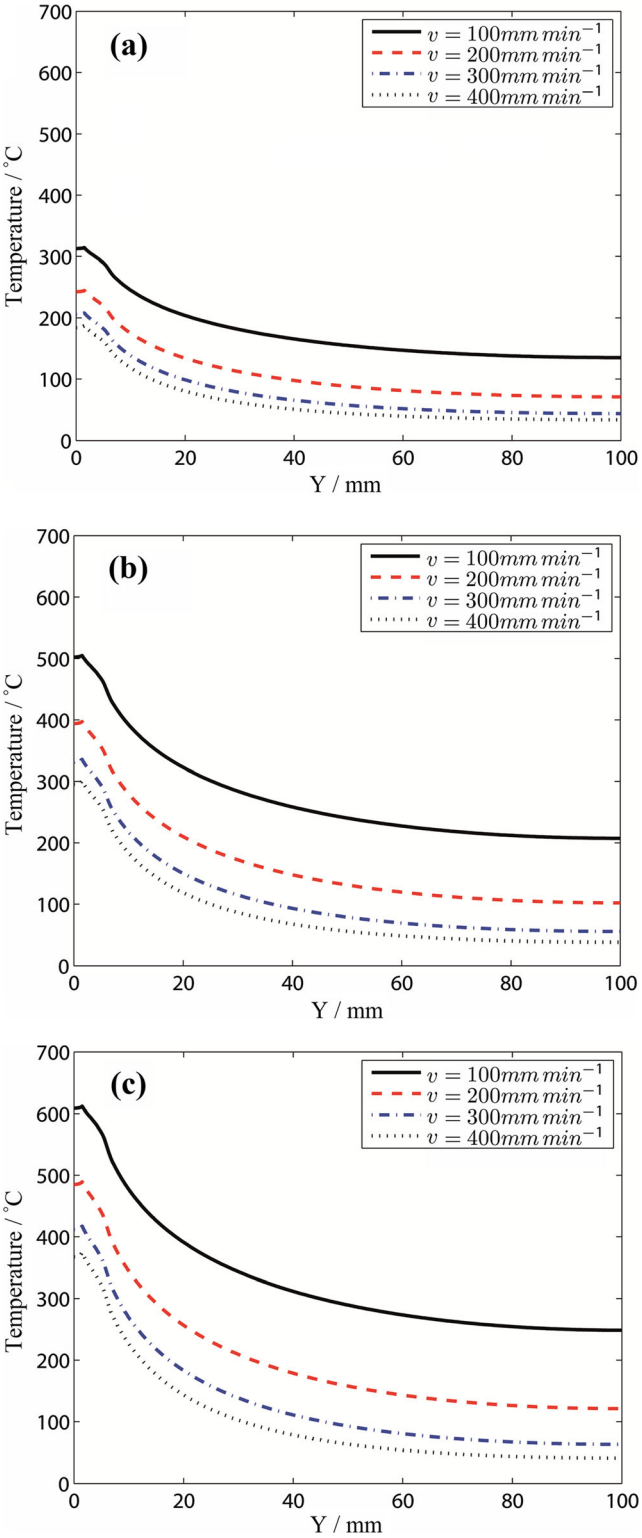

Fig. 5 Temperature distribution in *yz*-plane and along the *y*-direction, for different rotational speed of **a** 400 rev min^{-1}, **b** 700 rev min^{-1}, and **c** 900 rev min^{-1}

were annealed at 650 °C for 1 h before welding. The microstructure of the BM is presented in Fig. 3a. A simple cylindrical tool was made of H13 tool steel and used for FSW as illustrated in Fig. 3b. The pin diameter, shoulder diameter, and pin length were 3, 12, and 1.75 mm,

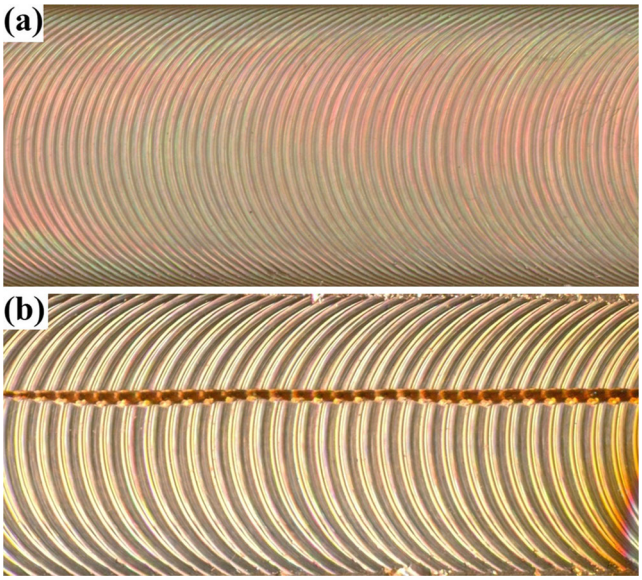

Fig. 6 **a** Surface of a defect-free joint welded at 900 rev min^{-1}–400 mm min^{-1}, **b** Surface of a joint with a tunnel type defect welded at 400 rev min^{-1}–400 mm min^{-1}

respectively. A conventional milling machine with 3° tilt degree of the tool relative to the work piece was used for conducting the experiments.

The plates were clamped firmly on the steel backplate, and then single pass butt FSW was conducted at different traverse speeds of 100, 200, 300, and 400 mm min^{-1} and various rotational speeds of 400, 700, and 900 rev min^{-1}. After visual inspection of the welded sample surfaces, the microstructural features were examined by the optical microscopy (OM). For this purpose, the metallographic samples cross-sectioned from the joints transverse to the welding direction, then polished and etched with a solution of 20 mL nitric acid and 10 mL acetic acid to disclose the microstructure. Average grain size in the SZ of the different joints was calculated by analyzing at least three images using Clemex image analysis software. This software differentiates dissimilar grains via a range of color contrast and then computes related diameter D_{Eq} of every grain from its area using the following equation [35]:

$$D_{Eq} = 1.2247\sqrt{\frac{4A}{\pi}} \tag{6}$$

where A is area (μm^2). The Vickers hardness test was conducted along the centerline on the traverse cross-section of the joints using a 100 g load for 10 s. Also, five tensile samples were prepared according to the ASTM: E8M standard and tensile tests were conducted at a cross head speed of 1 mm min^{-1}. Furthermore, type K thermocouples were used to quantify the temperatures during FSW at the bottom of the plates, exactly on the joint line.

3 Results and discussion

3.1 Temperature distributions

The results of simulation for the FSW of OFHC copper with different rotational speeds are illustrated in Fig. 4. As it can be seen, by increasing the rotational speed, the temperature diffusion in the weld width is increased due to the higher values of the generated heat. However, a closer look at the temperature profiles in the *yz*-plane (perpendicular to the traverse direction) shows that in the reduced traverse speed (no matter what the rotational speed is), the temperatures are quite distributed evenly, see Fig. 5.

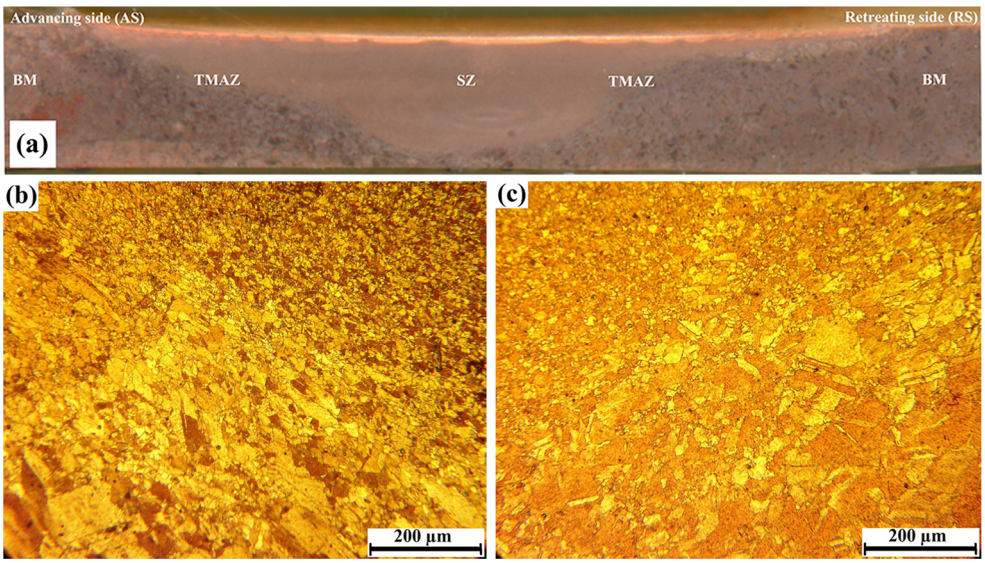

Fig. 7 **a** Typical macrostructure of a joint welded at 700 rev min^{-1}–200 mm min^{-1}, **b** and **c** microstructures of the TMAZ region at advancing side (*AS*) and retreating (*RS*), respectively

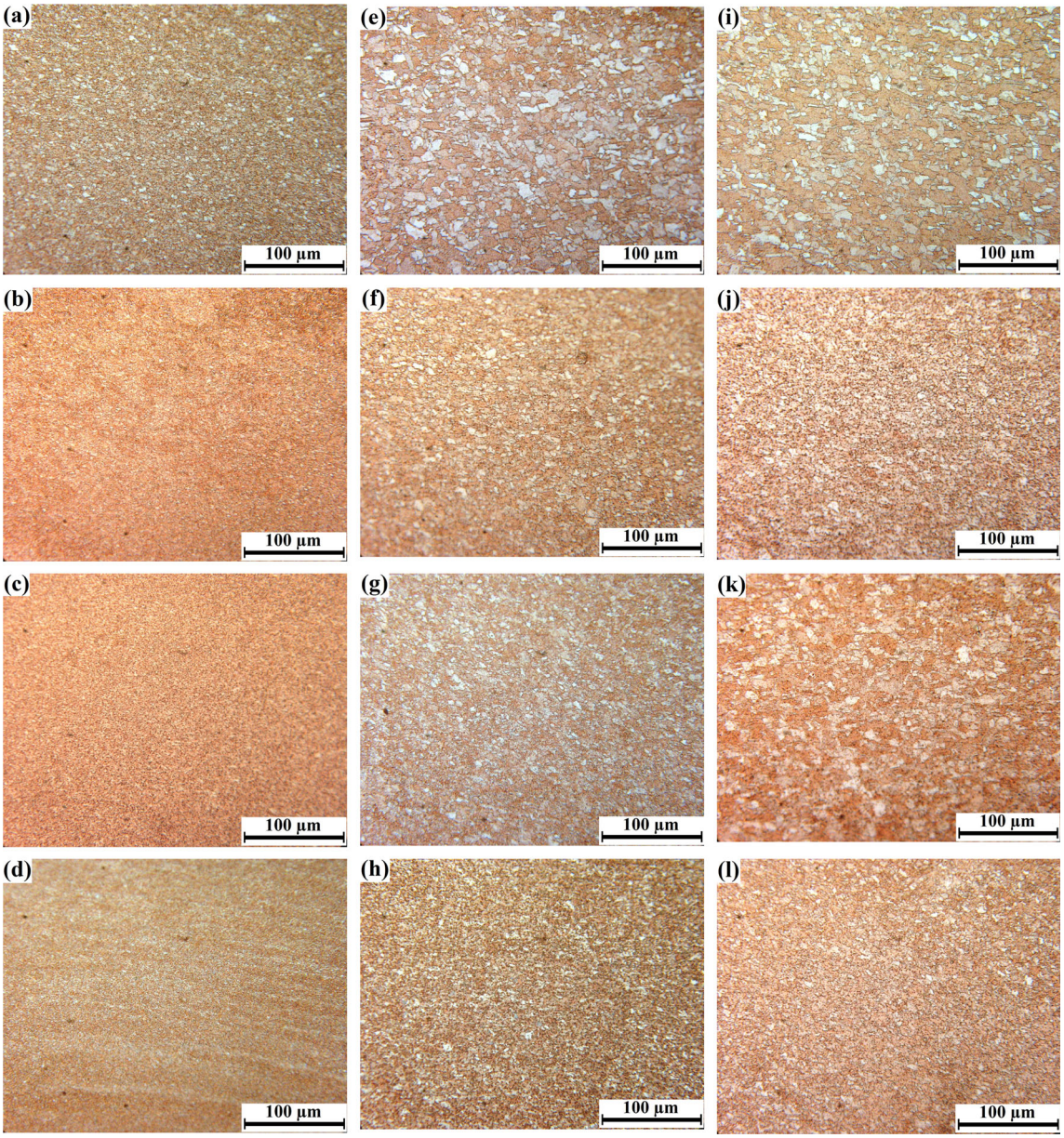

Fig. 8 The SZ microstructure of the joints welded at different rotational (rev min^{-1})–traverse (mm min^{-1}) speeds: **a** 400–100, **b** 400–200, **c** 400–300, **d** 400–400, **e** 700–100, **f** 700–200, **g** 700–300, **h** 700–400, **i** 900–100, **j** 900–200, **k** 900–300 and **l** 900–400

3.2 Macro- and microstructural characterization

Defect-free joints can be reached at all of the conducted rotational speeds of 400, 700, and 900 rev min^{-1}. However, it is notable that the tunnel defect form in joints welded at 400 rev min^{-1}–200 mm min^{-1}, 400 rev min^{-1}–300 mm min^{-1}, and 400 rev min^{-1}–400 mm min^{-1}. These defects are attributable to the combination of parameters: insufficient rotation speed combined with excessive traverse speed at constant axial force. In these cases, the welded parts cannot be properly stirred and mixed together, and hence a tunnel is created, running along the entire weld [19]. Therefore, it can be concluded that the rotation speed of 400 rev min^{-1} may not be a good parameter for producing defect-free joints. The surface of a defect-free joint and a tunnel type defect are illustrated in Fig. 6a and b, respectively.

A typical macrostructure of the joints with microstructural details is presented in Fig. 7. It reveals that the macrostructure of the joints consists of three different areas including SZ, thermo mechanically affected zone (TMAZ) and BM. The heat affected zone (HAZ) is not detectable in the welds due to high thermal conductivity of the OFHC copper.

The SZ microstructures welded at different conditions are shown in Fig. 8. Moreover, the average grain sizes of the SZ for the joints (d) are illustrated in Fig. 9a for both the experiments and the thermal model. According to Figs. 7a and 8,

the SZ of the joints have finer grain size compared to the BM. The coexistence of deformation and temperature during FSW cause to dynamic restoration phenomena such as dynamic recovery and recrystallization (DRV and DRX). Therefore, the fine and equiaxed microstructures in the SZ are the results of DRX. As seen from Fig. 9a, the average grain size increases with increasing the rotational speed (at a constant traverse speed). Furthermore, at a constant rotational speed, the higher traverse speeds lead to smaller SZ grain sizes. It has been demonstrated that the grain size of the SZ is affected mainly by two thermomechanical factors including degree of deformation and peak temperature during FSW [9]. Higher rotational speeds (at constant traverse speed) cause to higher deformation degrees and peak temperatures, while higher traverse speeds (at constant rotational speed) lead to lower ones. Additionally, increase in degree of deformation and decrease in peak temperature result in finer SZ grain sizes. Thus, it can be concluded that in this study the dominant factor is peak temperature of the SZ during FSW. The SZ peak temperatures (T_{max}) determined by both numerical modeling and experimental result are shown in Fig. 9b. As it is seen from Fig. 9a, b, the numerical modeling and experimental results are in good agreement. However, there is a little difference between them, since the mechanical deformation and

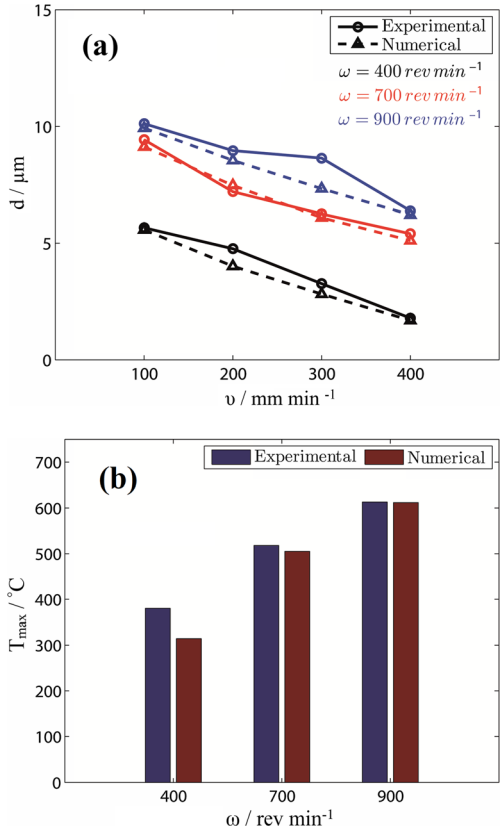

Fig. 9 **a** Predicted and measured grain size for all test cases, and **b** predicted and measured pick temperature of the SZ for different rotational speed with the traverse speed of 100 mm min^{-1}

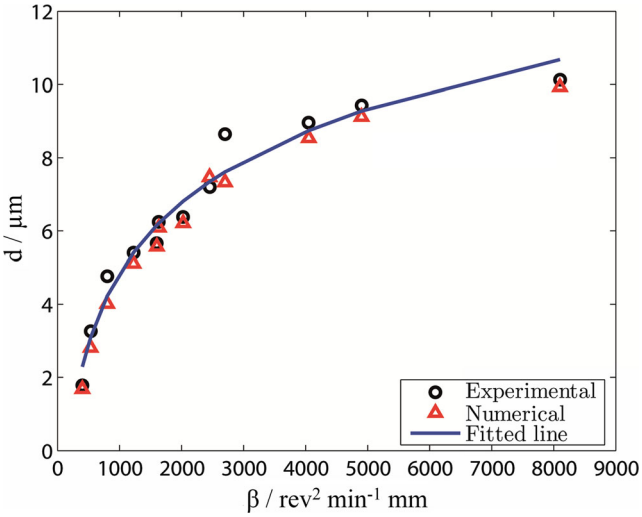

Fig. 10 Influence of β on the predicted and measured grain size (d)

the resultant heat generation in the developed thermal model has been neglected.

Recently, some investigators have shown that ω^2/υ ratio (which we call it here as β) has a considerable effect on the SZ peak temperature and corresponding grain size during FSW of different alloys [35, 36]. For example, Commin et al. [36] established a relationship between the SZ temperature (T) and the process parameter (ω, υ) for aluminum alloys as follows:

$$\frac{T}{T_m} = k^2 \left(\frac{\omega^2}{10^4 \cdot \upsilon} \right)^{\alpha} \tag{7}$$

where T_m is the alloy melting point, and the constants α and K can respectively vary between 0.04–0.06 and 0.65–0.75 [37]. The influence of the different ω^2/υ ratio (β) on the produced

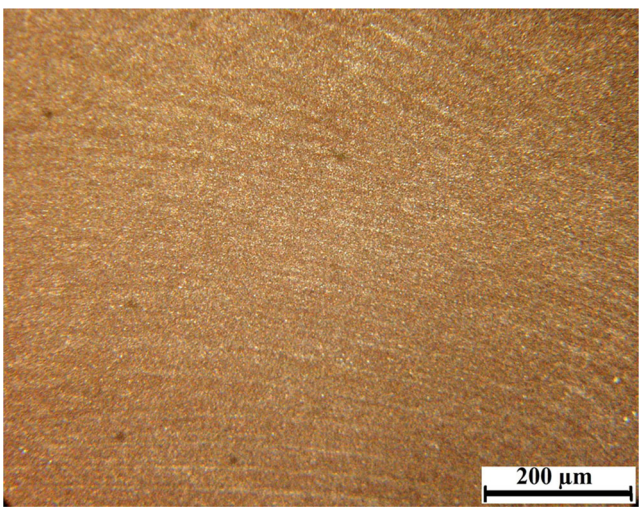

Fig. 11 Low magnification of the SZ microstructure in the joint welded at 400 rev min^{-1}–400 mm min^{-1}, revealing the onion rings

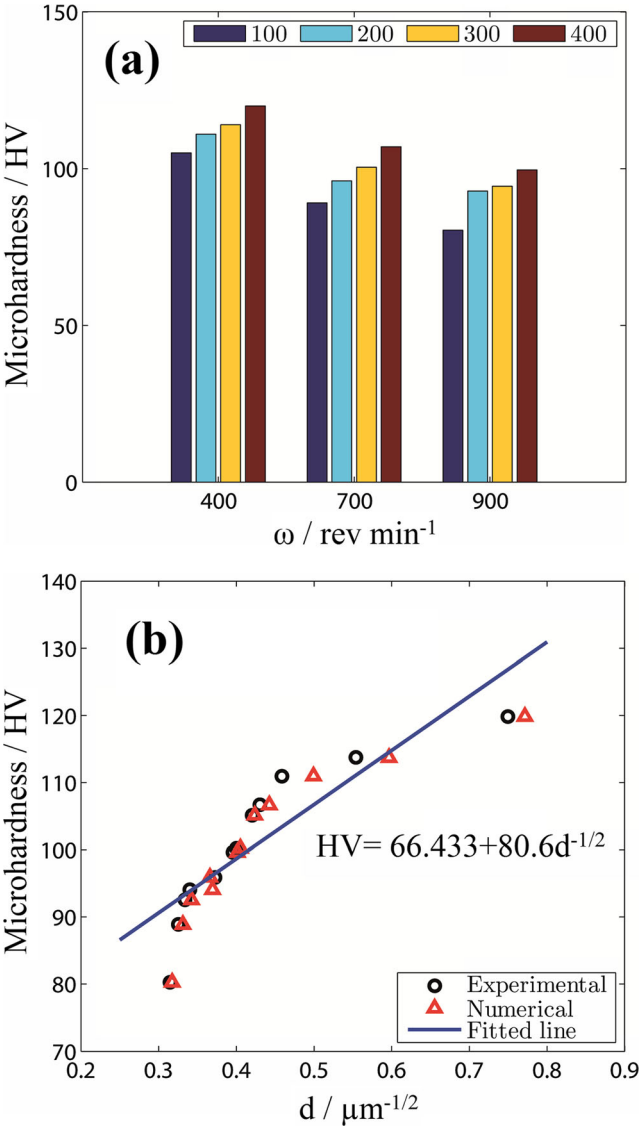

Fig. 12 **a** The average microhardness of the SZ for the different welding conditions, **b** the average microhardness of the SZ vs. the reciprocal of the square root of the grain size

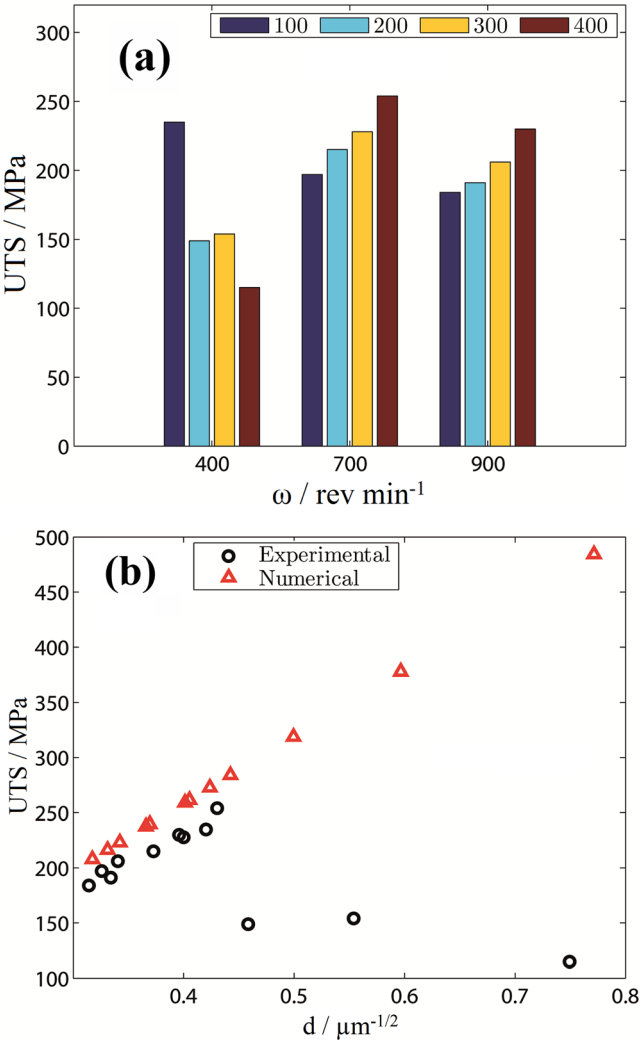

Fig. 13 **a** Ultimate tensile strength of the joints welded at different conditions, and **b** correlation between the average grain size and UTS

grain size (which in essence can be correlated to the peak temperature of the SZ) for the different FSW conditions are illustrated in Fig. 10. From Eq. 7, it is notable that higher ω^2/υ ratio produces higher peak temperature. As a consequence, the grain size of the SZ will increase which is shown in Fig. 10 for both experiments and the thermal model. The critical temperature for the dynamic recrystallization, deformation temperature (T), and the strain rate ($\dot{\varepsilon}$) are related by the Zener-Hollomon parameter (Z) equation [36]:

$$Z = \dot{\varepsilon}\exp\left(\frac{Q}{RT}\right) \tag{8}$$

where, Q is activation energy, R is the gas constant. In addition, the relationship between dynamically recrystallized grain size (d) and Z during thermomechanical processes of alloys can be stated by the equation [38]:

$$d = aZ^b \tag{9}$$

where a and b are constants. For dynamic recrystallization, the exponent b usually has a negative amount. By substituting Eq. 8 into Eq. 9 and then taking the natural logarithm, the resulted formula will be as follows:

$$\ln d = \ln a + b\ln\left(\dot{\varepsilon}\exp\left({}^{Q}/_{RT}\right)\right) \tag{10}$$

According to Eq. 7, the SZ temperature is a function of ω and υ amounts, as higher ω and lower υ result in higher temperatures, respectively. Also, based on this equation, the

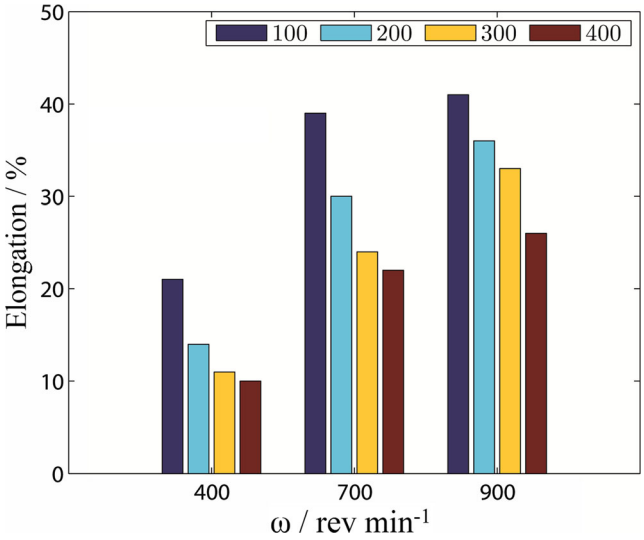

Fig. 14 Tensile elongation of the joints welded at different conditions

effect of ω (with exponent of 2) is more than that of υ (with exponent of 1). The impact of ω on the microstructural and mechanical properties during FSW of pure copper has been emphasized by some researchers [19]. From Eq. 10, it can be concluded that higher SZ temperatures (higher ω and lower υ) cause lower amounts of Z and hence higher d amounts.

One of the microstructural features that have been detected in this investigation is onion rings. The formation of the onion rings can be elucidated by different reasons such as the geometrical effect, the differences in grain size, and the particle-rich bands [4]. The SZ microstructure of the joints (Fig. 8) reveals that the onion rings in this study appear at the lowest peak temperature or heat input condition (i.e., for the joint welded at 400 rev min^{-1} and 400 mm min^{-1}). The onion rings shown in Fig. 8d is illustrated at lower magnification in Fig. 11. For other FSW conditions, the onion rings vanished. The origin of the onion rings cannot be related to the particle-rich bands due to absence of particles in the BM. Hence, it is suggested that this phenomena is associated with variation of grain sizes, which are formed because of inadequate deformation or different amount of deformation experienced by the material at very low heat input condition.

3.3 Mechanical properties

The variation of the average microhardness of the SZ for the joints is illustrated in Fig. 12a. As seen, the lower rotational speed and higher traverse speed cause to higher hardness values in the SZ of the joints. The grain size of the SZ, which was predicted by thermal model and measured from the experiments are correlated to the microhardness values. The result of such correlation between the average microhardness of the SZ of different joints is plotted vs. the reciprocal of the square root of the grain size in Fig. 12b. It is seen that the hardness distribution in the SZ follows the Hall-Petch relationship. Accordingly, the Hall-Petch linear relationship can be presented as follows:

$$\mathrm{HV} = 66.433 + 80.6 \times d^{-1/2} \tag{11}$$

where HV is the average microhardness of the SZ, and d is average grain size of the SZ. Equation 11 confirms that the finer grain size causes higher hardness, as the finer grains

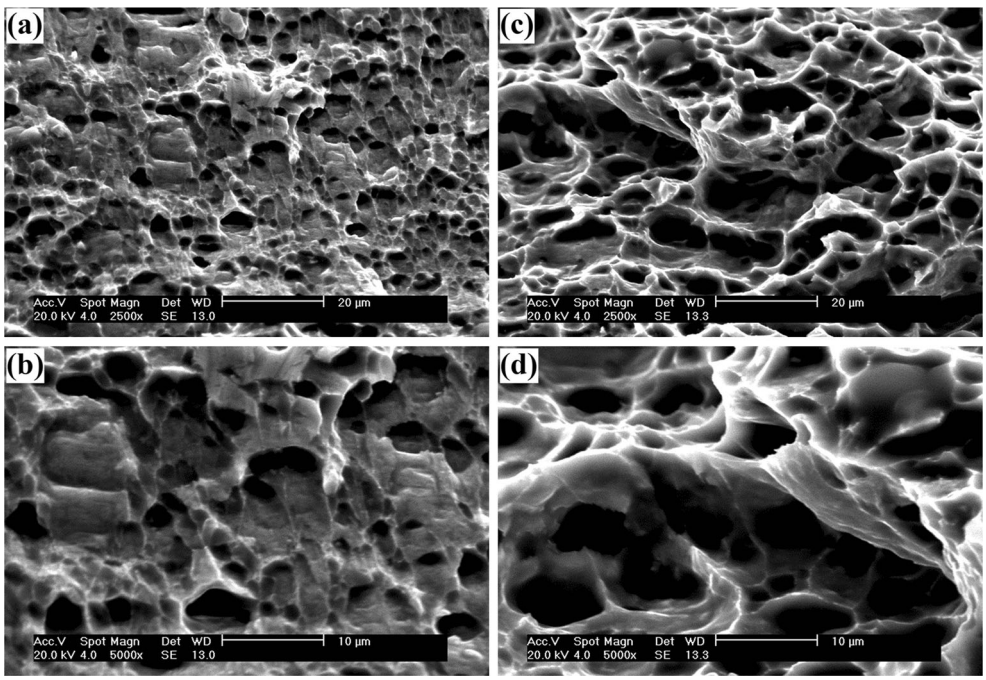

Fig. 15 SEM fractographs of tensile specimens welded at: **a** and **b** lower peak temperatures (700 rev min^{-1}–400 mm min^{-1}), **c** and **d** higher peak temperatures (900 rev min^{-1}–100 mm min^{-1})

consist of more grain boundaries, which are the major hindrances to the dislocation slips [35].

The ultimate tensile strength (UTS) variation of the joints produced by FSW with different process parameters are illustrated in Fig. 13a. It can be seen that by increasing the rotational speed from 400 to 700 rev min^{-1} for each of the traverse speeds, the UTS of the joints will increase (neglecting the UTS value for the case 400 rev min^{-1}–100 mm min^{-1}). From the experimental view point, this is the region where the recrystallization of the grains occurs and the finer grains promote better mechanical properties. However, by further increase of the rotational speed from 700 to 900, the UTS values of the joints will decrease. This is attributed to the grain growth of the recrystallized grain due to the generated heat [20]. At FSW conditions of 400 rev min^{-1}–200 mm min^{-1}, 400 rev min^{-1}–300 mm min^{-1} and 400 rev min^{-1}–400 mm min^{-1}, the defects form in the joints which cause to lower UTS. Formation of defects is attributed to the inadequate heat generation and plastic flow during FSW [19]. Moreover, according to the previous results shown in the present study, higher traverse speeds results in lower heat input conditions (lower peak temperatures in Fig. 9b), lower grain sizes (Fig. 9a), and hence higher UTS.

The predicted values for the grain size can be converted to the UTS values using the Hall-Petch relation [32], and knowing that UTS=(1.1–1.3) YS [39]. This leads to a semi-empirical relation for the numerical correlation between the grain size and the UTS shown in Eq. 12. The comparison between the numerical results and the experimental one is shown in Fig. 13b.

$$\mathrm{UTS} = 1.17 \times \left(12.77 + 520 \times d^{-1/2}\right) \tag{12}$$

Figure 14 shows the effect of rotational and traverse speeds on the tensile elongation (TE) of the joints. Seen from Fig. 14, an increase in the rotational speed will cause to increase in TE of the joints continuously where the decrease in traverse speed results in the increase in TE. Higher rotational speeds and lower traverse speeds lead to removal of the defects in the joints and hence higher TE. Also, increasing the rotational speed and decreasing the traverse speed produces enough heat for metallurgical transformations such as grain coarsening, growth of participates, and lowering of dislocation density at SZ of the joints [18–20]. In this study, according to Fig. 9a, b, higher peak temperatures lead to coarser final grain sizes. Furthermore, higher peak temperatures may result in lower dislocation densities, and thus higher TE. This statement has been supported by SEM fractography of the tensile samples. As designated in Fig. 15, the higher peak temperatures during FSW result in more dimples and fewer large voids (Fig. 15c, d) in the fracture surface compared to lower peak temperatures (Fig. 15a, b).

4 Conclusions

A thermal model was developed to predict the grain size and mechanical properties of the friction stir welded OFHC pure copper joints, and the following results are achieved from numerical and experimental results:

1. Defect-free joints can be achieved at different FSW conditions except for very low heat input conditions, i.e., 400 rev min^{-1}–200 mm min^{-1}, 400 rev min^{-1}–300 mm min^{-1}, and 400 rev min^{-1}–400 mm min^{-1}.
2. The numerical and experimental results for the grain size of the joints are in a good agreement. The results show that higher rotational speed and lower traverse speed cause to higher peak temperature, and hence higher grain size. Consequently, the peak temperature was the dominant factor controlling the grain size of the joints.
3. The hardness distribution in the SZ follows the Hall-Petch relationship. Finer grain sizes lead to higher hardness of the joints.
4. In the case of the UTS, the numerical results are in agreement with experimental ones for defect-free joints, and UTS of the joints increase with decreasing the grain size. For defective joints, the numerical results are higher than the experimental ones, because defect formation is not considered in the model.
5. Higher rotational speeds and lower traverse speeds, or higher heat input conditions, cause to increase TE of the joints. The fracture surfaces of the joints welded at higher heat input conditions reveal more dimples and fewer large voids compared to the joints welded at lower heat input conditions.

Acknowledgments The authors acknowledge use of the services and facilities of the Welding Center at the Sahand University of Technology. Dr. Tohid Saeid is gratefully acknowledged for his constructive discussions through the project.

References

1. Shen JJ, Liu HJ, Cui F (2010) Effect of welding speed on microstructure and mechanical properties of friction stir welded copper. J Mater Des 31:3937–3942. doi:10.1016/j.matdes.2010.03.027
2. Xue P, Xie GM, Xiao BL, Ma ZY, Geng L (2010) Effect of heat input conditions on microstructure and mechanical properties of friction-stir-welded pure copper. Metall Mater Trans A 41:2010–2021. doi:10.1007/s11661-010-0254-y

3. Nandan R, DebRoy R, Bhadeshia HKDH (2008) Recent advances in friction stir welding-process, weldment structure and properties. Prog Mater Sci 53:980–1023. doi:10.1016/j.pmatsci.2008.05.001
4. Xie GM, Ma ZY, Geng L (2007) Development of a fine-grained microstructure and the properties of a nugget zone in friction stir welded pure copper. Scripta Mater 57:73–76. doi:10.1016/j.scriptamat.2007.03.048
5. Surekha K, Els-Botes A (2011) Development of high strength, high conductivity copper by friction stir processing. J Mater Des 32:911–916. doi:10.1016/j.matdes.2010.08.028
6. Sakthivel T, Mukhopadhyay J (2007) Microstructure and mechanical properties of friction stir welded copper. J Mater Sci 42:8126–8129. doi:10.1007/s10853-007-1666-y
7. Sun YF, Fujii H (2010) Investigation of the welding parameter dependent microstructure and mechanical properties of friction stir welded pure copper. J Mater Des 527:6879–6886. doi:10.1016/j.msea.2010.07.030
8. Lee W, Jung S (2004) The joint properties of copper by friction stir welding. Mater Lett 58:1041–1046. doi:10.1016/j.matlet.2003.08.014
9. Liu HJ, Shen JJ, Huang YX, Kuang LY, Liu C, Li C (2009) Effect of tool rotation rate on microstructure and mechanical properties of friction stir welded copper. Sci Technol Weld J 14:577–583. doi:10.1179/136217109X456951
10. Cederqvist L, Sorensen CD, Reynolds AP, Oberg T (2009) Improved process stability during friction stir welding of 5 cm thick copper canisters through shoulder geometry and parameter studies. Sci Technol Weld J 14:178–184. doi:10.1179/136217109X400420
11. Leal RM, Sakharova N, Vilaa P, Rodrigues DM, Loureiro A (2011) Effect of shoulder cavity and welding parameters on friction stir welding of thin copper sheets. Sci Technol Weld J 16:146–152. doi:10.1179/1362171810Y.0000000005
12. Farrokhi H, Heidarzadeh A, Saeid T (2013) Friction stir welding of copper under different welding parameters and media. Sci Technol Weld J 18:697–702. doi:10.1179/1362171813Y.0000000148
13. Teimournezhad J, Masoumi A (2010) Experimental investigation of onion ring structure formation in friction stir butt welds of copper plates produced by non-threaded tool pin. Sci Technol Weld J 15:166–170. doi:10.1179/136217109X12577814486610
14. Savolainen K, Saukkonen T, Hanninen H (2012) Banding in copper friction stir weld. Sci Technol Weld J 17:111–115. doi:10.1179/1362171811Y.0000000089
15. Khodaverdizadeh H, Heidarzadeh A, Saied T (2013) Effect of tool pin profile on microstructure and mechanical properties of friction stir welded pure copper joints. J Mater Des 45:265–270. doi:10.1016/j.matdes.2012.09.010
16. Rajakumar S, Muralidharan C, Balasubramanian V (2010) Establishing empirical relationships to predict grain size and tensile strength of friction stir welded AA 6061-T6 aluminum alloy joints. T Nonferr Metal Soc 20:1863–1872. doi:10.1016/S1003-6326(09)60387-3
17. Rajakumar S, Muralidharan C, Balasubramanian V (2011) Predicting tensile strength, hardness and corrosion rate of friction stir welded AA6061-T6 aluminum alloy joints. J Mater Des 32:2878–2890. doi:10.1016/S1003-6326(09)60387-3
18. Heidarzadeh A, Mahmoudi A, Khodaverdizadeh H, Nazari E (2012) Tensile behavior of friction stir welded AA 6061-T4 aluminum alloy joints. J Mater Des 37:166–173. doi:10.1016/j.matdes.2011.12.022
19. Heidarzadeh A, Saeid T, Khodaverdizadeh H, Mahmoudi A, Nazari E (2013) Establishing a mathematical model to predict the tensile strength of friction stir welded pure copper joints. Metall Mater Trans B 44B:175–183. doi:10.1007/s11663-012-9755-y
20. Heidarzadeh A, Saeid T (2013) Prediction of mechanical properties in friction stir welds of pure copper. J Mater Des 52:1077–1087. doi:10.1016/j.matdes.2013.06.068
21. Rajakumar S, Balasubramanian V (2012) Establishing relationships between mechanical properties of aluminum alloys and optimised friction stir welding process parameters. J Mater Des 40:17–35. doi:10.1016/j.matdes.2012.02.054
22. Elangovan K, Balasubramanian V, Babu S (2009) Predicting tensile strength of friction stir welded AA6061 aluminum alloy joints by a mathematical model. J Mater Des 30:188–193. doi:10.1016/j.matdes.2008.04.037
23. Colligan K (1999) Material flow behavior during friction stir welding of aluminum. Suppl Weld J 5:229–237
24. Li Y, Murr L, McClure JC (1999) Solid state flow visualization in the friction stir welding of 2024 Al to 6061 Al. Scripta Mater 40:1041–1046. doi:10.1016/S1359-6462(99)00062-7
25. Guerra M, Schmidt C, McClure JC, Murr LE, Nunes A (2003) Flow patterns during friction stir welding. Mater Charact 49:95–101. doi:10.1016/S1044-5803(02)00362-5
26. Schmidt HNB, Dickerson TL, Hattel JH (2006) Material flow in butt friction stir welds in AA2024-T3. Acta Mater 54:1199–1209. doi:10.1016/j.actamat.2005.10.052
27. Russell MJ, Shercliff HR, Proc. 1st Int. Symp (1999) On 'Friction Stir Welding'. TWI, California
28. Schmidt H, Hattel J, Wert J (2004) An analytical model for heat generation in friction stir welding. Model Simul Mater Sci Eng 12:143–157. doi:10.1088/0965-0393/12/1/013
29. Schmidt HB, Hattel JH (2008) Thermal modelling of friction stir welding. Scripta Mater 58:332–337. doi:10.1016/j.scriptamat.2007.10.008
30. Soundararajan V, Zekovic S, Kovacevic R (2005) Thermo-mechanical model with adaptive boundary conditions for friction stir welding of Al 6061. Int J Mach Tools Manu 45:1577–1587. doi:10.1016/j.ijmachtools.2005.02.008
31. Sonne MR, Tutum CC, Hattel JH, Simar A, Meester B (2013) The effect of hardening laws and thermal softening on modeling residual stresses in FSW of aluminum alloy 2024-T3. J Mater Process Technol 213:477–486. doi:10.1016/j.jmatprotec.2012.11.001
32. Song M, Kovacevic R (2003) Thermal modeling of friction stir welding in a moving coordinate system and its validation. Int J Mach Tools Manu 43:605–615. doi:10.1016/S0890-6955(03)00022-1
33. Prasad YVRK, Sasidhara S (1997) Hot working guide: a compendium of processing maps. ASM International, Ohio
34. Harper JME, Cabral C Jr, Andricacos PC, Gignac L, Noyan IC, Rodbell KP, Hu CK (1999) Mechanisms for microstructure evolution in electroplated copper thin films near room temperature. J Appl Phys 86:2516–2525. doi:10.1063/1.371086
35. Motalleb-nejad P, Saeid T, Heidarzadeh A, Darzi K, Ashjari M (2014) Effect of tool pin profile on microstructure and mechanical properties of friction stir welded AZ31B magnesium alloy. J Mater Des 59:221–226. doi:10.1016/j.matdes.2014.02.068
36. Commin L, Dumont M, Masse JE, Barrallier L (2009) Friction stir welding of AZ31 magnesium alloy rolled sheets: influence of processing parameters. Acta Mater 57:326–334. doi:10.1016/j.actamat.2008.09.011
37. Arora A, De A, Debroy T (2011) Toward option friction stir welding tool shoulder diameter. Scripta Mate 64:9–12. doi:10.1016/j.scriptamat.2010.08.052
38. Polar A, Indacochea JE (2009) Microstructural assessment of copper friction stir welds. J Manuf Sci E 131:1–7. doi:10.1115/1.3123313
39. Krishna SC, Gangwar NK, Jha AK, Pant B (2013) On the prediction of strength from hardness for copper alloys. J Mater :1–6. doi:10.1155/2013/352578